

# We are IntechOpen, the world's leading publisher of Open Access books Built by scientists, for scientists

6,900

Open access books available

186,000

International authors and editors

200M

Downloads

Our authors are among the

154

Countries delivered to

TOP 1%

most cited scientists

12.2%

Contributors from top 500 universities



WEB OF SCIENCE™

Selection of our books indexed in the Book Citation Index  
in Web of Science™ Core Collection (BKCI)

Interested in publishing with us?  
Contact [book.department@intechopen.com](mailto:book.department@intechopen.com)

Numbers displayed above are based on latest data collected.  
For more information visit [www.intechopen.com](http://www.intechopen.com)



# Electronic States of Graphene-Based Ferromagnets

Masashi Hatanaka

*Department of Green and Sustainable Chemistry,  
School of Engineering, Tokyo Denki University,  
2-2 Kanda Nishiki-cho, Chiyoda-ku, Tokyo  
Japan*

## 1. Introduction

Graphenes have attracted many physicists and/or chemists because of the beautiful structure and tunable electronic states. One of the remarkable properties is the high carrier mobility due to the famous Dirac point, in which the effective mass is theoretically zero (Novoselov, et al., 2004, 2005). The motion of electrons is described by pseudo relativistic effect, and new aspects on physics and chemistry of two-dimensional systems have been developed as nano-scale technology. Nowadays, there has been increasing interest of modified graphenes toward thin films, nano particles, adsorbance agents, and so on, as well as possible micro-electronic devices.

On the other hand, magnetism of graphenes is another interesting theme, related to the early studies on so-called graphene ribbons. That is, some graphene derivatives are promising candidates for organic ferromagnets. The magnetic properties depend on topological conditions such as edges, pores, and defects. Toward a new type of ferromagnets, chemical modification of graphene is a highly challenging theme. Paramagnetism of graphitic polymers itself has been theoretically predicted, relating to the edge states, pores, and defects. However, it was not until band structures of modified graphenes revealed the existence of flat bands at the frontier levels that robust ferromagnetism has been highly expected from graphene-based skeletons. The edges, pores, and defects in these systems should be ordered so as to cause completely flat bands in the Hückel level. Hückel analysis on modified graphenes gives a good perspective toward the flat-band ferromagnetism. In this chapter, graphene-based ferromagnetism is analyzed by crystal orbital method. Recent advances in magnetic graphenes are reviewed in view of their electronic states.

## 2. Methylene-edged graphenes

It is well known that graphene ribbons with peculiar type of edges have polyradical character, of which flat bands cause ferromagnetic interactions. Fig. 1 shows three types of graphene ribbons. Fig. 1a is the famous graphene ribbons with two-sided acene (zigzag) edges. The magnetic ordering has been predicted based on the band structures. The HOCO (highest occupied crystal orbital) and LUCO (lowest unoccupied crystal orbital) contact and become flat at the wavenumber region  $|k| > 2\pi/3$  (Fujita et al., 1996). Thus, at least within

the same edge, ferromagnetic interactions are expected. However, total magnetism in the acene-edged graphene ribbons is probably small, because spin moments at both sides tend to cancel each other. This is intuitively deduced from the conventional Heisenberg model. To avoid the spin-cancellation, hydrogen, oxygen and fluorine passivations have been suggested (Kusakabe & Maruyama, 2003; Maruyama & Kusakabe, 2004).

Instead, Klein suggested methylene-edged graphene ribbons shown in Fig. 1b (Klein, 1994; Klein & Bytautas, 1999). Nowadays, these are called Klein edges. At least within the same edge, the Klein-edged graphenes are also expected to show ferromagnetic interactions due to the flatness of frontier bands at  $|k| < 2\pi/3$  (not  $|k| > 2\pi/3$ ). In this case, however, spin cancellation is also expected due to spin alternation in the bipartite lattice. While two-sided Klein edges cause spin cancellation, one-sided Klein edges shown in Fig. 1c are expected to show robust ferromagnetic interactions, because ferrimagnetic spin-polarized structures can be drawn by classical valence-bond theory. Although some studies predicted the antiferromagnetic states of the one-sided Klein edges with twisted or partially substituted methylene groups (Maruyama & Kusakabe, 2004), conservation of the planarity probably makes them ferromagnetic non-Kekulé polymers, and the electronic states are described by Wannier functions rather than conventional Bloch functions (Hatanaka, 2010a). Then, there appears one non-bonding band at the frontier level. The non-bonding band is completely flat within the Hückel approximation. Each Wannier function spans common atoms between the adjacent cells. This is necessary and sufficient condition for ferromagnetic interactions in conjugated  $\pi$  systems, similar to triplet biradicals. Non-cancelled spin alignment and itinerant ferromagnetism are expected due to the flat band.

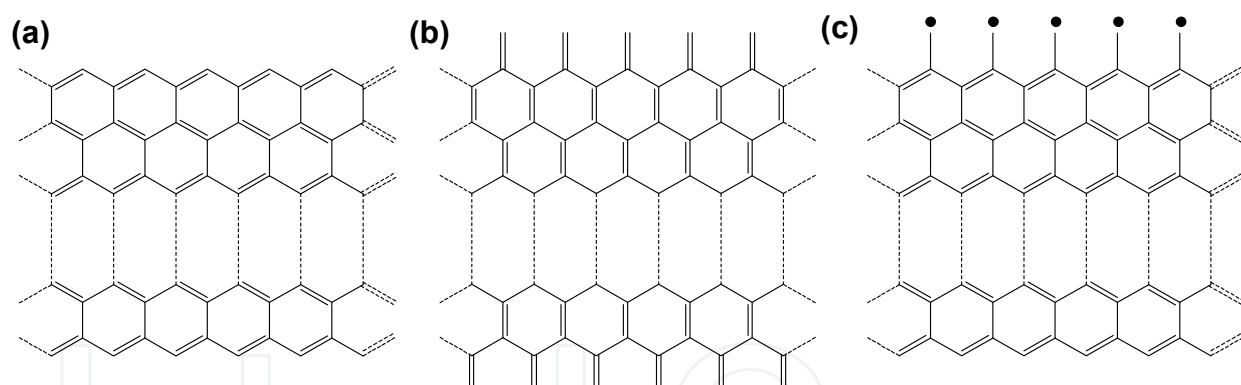


Fig. 1. Graphenes with (a) acene (zigzag)-, (b) two-sided Klein-, and (c) one-sided Klein edges.

For simplicity, we first consider a small non-Kekulé polymer shown in Fig. 2. There are non-bonding crystal orbitals (NBCOs) at the frontier level. They are completely degenerate under Hückel approximation. Each NBCO can be transformed into Wannier functions localized around each cell, as formulated below.

We consider Bloch functions corresponding to the NBCO band:

$$\varphi_k = \frac{1}{\sqrt{N}} \sum_{\mu}^N \sum_r^{cell} \exp(ik\mu) C_r(k) \chi_{\mu,r}, \quad (1)$$

where the wavenumber  $k$  runs from  $-\pi$  to  $\pi$ ,  $\mu$  is the cell index,  $N$  is the number of cells, and  $r$  is the index of atomic orbitals. Here we adopt the real part of  $C_r(k)$ :

$$C'_r(k) = \frac{1}{2} \{C_r(k) + C_r(k)^*\} = \frac{1}{2} \{C_r(k) + C_r(-k)\}. \quad (2)$$

This procedure minimizes the exchange integral of the system. The Wannier function localized at the  $\nu$ -th cell is expressed by Equations (3) and (4):

$$\psi_\nu = \sum_{\mu}^N \sum_r^{cell} a_r(\mu - \nu) \chi_{\mu,r}, \quad (3)$$

$$a_r(\mu - \nu) = \frac{1}{2\pi} \int_{-\pi}^{\pi} \exp\{i(\mu - \nu)k\} C'_r(k) dk, \quad (4)$$

where

$$\tau = \mu - \nu. \quad (5)$$

Each Wannier coefficient is a function of the integer  $\tau$ , which represents the difference from the  $\nu$ -th cell. The Wannier functions should be normalized using a proper normalization factor, because the linear combinations of Bloch coefficients in Equation (2) are not always normalized to unity. Under Hückel approximation, the normalization factor is:

$$C' = \frac{1}{\sqrt{\sum_{\tau} \sum_r |a_r(\tau)|^2}}. \quad (6)$$

Wannier functions in the original paper are not normalized (Hatanaka, M. & Shiba, R., 2007; Hatanaka, 2010a). In the present review, however, we adopt the renormalized Wannier functions, and the exchange integrals are recalculated. Since each Wannier function coefficient  $a_r(\tau)$  localizes at one or a few unit cells around the  $\nu$ -th cell,  $a_r(\tau)$  with  $|\tau| \geq 2$  can be ignored. Then, the exchange integral  $K_{ij}$  between the  $i$ -th and  $j$ -th Wannier functions is nontrivial only when  $|i-j| = 1$ :

$$\begin{aligned} K_{ij} &= \iint \psi_i(\mathbf{1}) \psi_j(\mathbf{1}) \frac{e^2}{r_{12}} \psi_i(\mathbf{2}) \psi_j(\mathbf{2}) d\tau_1 d\tau_2 \\ &\cong \sum_r \sum_s \sum_t \sum_u a_r(i) a_s(j) a_t(i) a_u(j) (rs|tu) \\ &\cong \left\{ \sum_r^{i-th \text{ cell}} \{a_r(0)^2 a_r(-1)^2\} + \sum_r^{j-th \text{ cell}} \{a_r(0)^2 a_r(1)^2\} \right\} (rr|rr) \\ &\propto 2 \sum_r^{i-th \text{ cell}} \{a_r(0)^2 a_r(1)^2\}, \end{aligned} \quad (7)$$

where  $(rs|tu)$  denotes the electron-repulsion integrals, and only one-centered integrals were taken into account in the approximation. The last expression results from Equation (2). From Equation (7), the exchange integrals of non-bonding extended systems are deduced from the amplitude pattern of their Wannier functions. The Bloch and Wannier functions can be calculated by usual secular equations and numerical integrals (Hatanaka, M. & Shiba, R., 2007).

The  $\nu$ -th Wannier function  $\psi_\nu$  is schematically shown in Fig. 2. In general, Wannier functions decay rapidly with increase in distance from the central cell. However, in this case, we see

that the  $\nu$ -th and  $(\nu+1)$ -th Wannier functions span common atoms between the adjacent region. Then, the two-electron wavefunction  $\psi_\nu\psi_{\nu+1}$  contains so-called ionic terms, in which two electrons are accommodated to the same atomic orbitals. While simultaneous occupation of two electrons with antiparallel spins is allowed in the same atomic orbital, occupation of electrons with parallel spins is forbidden due to the Pauli principle. Thus, in this system, high-spin state is preferred rather than low-spin state due to reduction of Coulomb repulsion.

Klein-edged graphenes with  $n$  ladders are similarly analyzed as non-Kekulé polymers, as shown in Fig. 3. In these systems, amplitudes of the Wannier functions are mainly spread at upper and lower edges. When the number of ladders  $n$  increases, the amplitudes inside the graphene plane become small, and highly localize at the edges. Nevertheless, even if the number of ladders becomes infinite, each Wannier function spans common atoms between the adjacent cells, and thus, the ferromagnetic interactions are always positive. This means that the high-spin stabilities are attributed to itinerant character of edge states, which is described by the Wannier functions. Nowadays, it has been theoretically shown that the Wannier functions in such degenerate systems should be symmetric with respect to the central cell, and minimize the exchange integral of the systems (Hatanaka, 2011). Then, the exchange integral is calculated from square of the amplitude pattern of the two-electron wavefunction  $\psi_\nu\psi_{\nu+1}$ , as schematically shown in Fig. 4. The exchange integral  $K$  versus the number of ladders  $n$  is shown in Fig. 5. The exchange integral is calculated from the Wannier coefficients, taking count of one-centered integrals. The exchange integral converges to a positive value, and thus, the system is expected to be ferromagnetic in the bulk order. For chemical stability, carbonyl edges isoelectronic with methylene groups are promising.

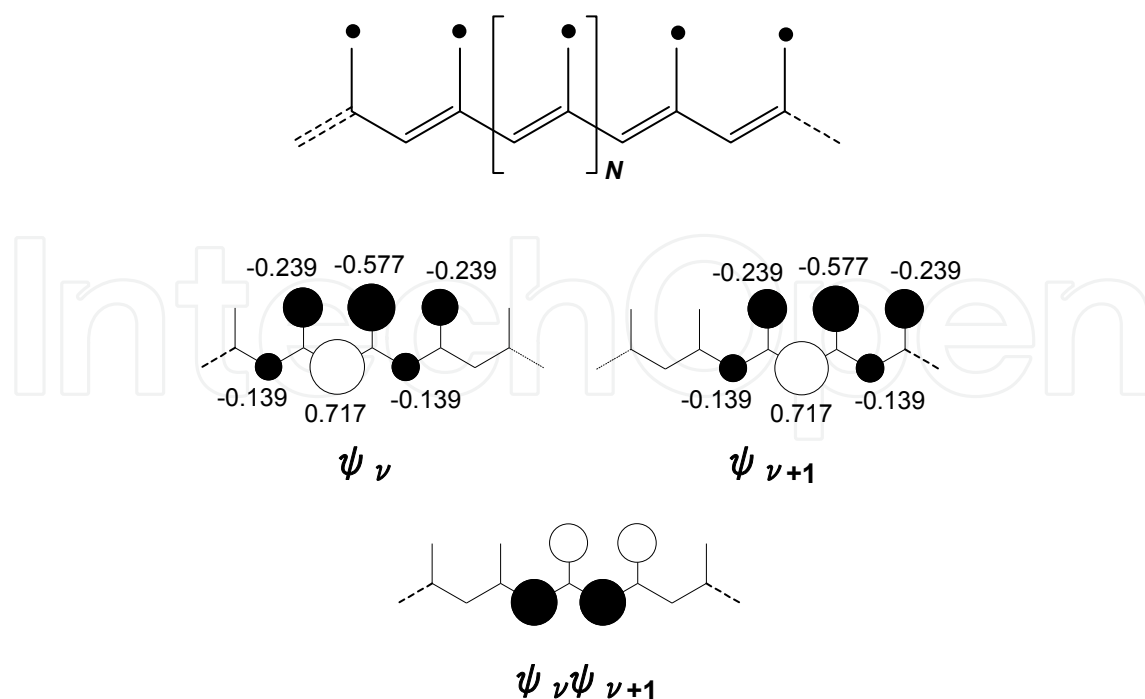


Fig. 2. Wannier functions of the simplest non-Kekulé polymer. This is a simple model for Klein-edged graphenes.

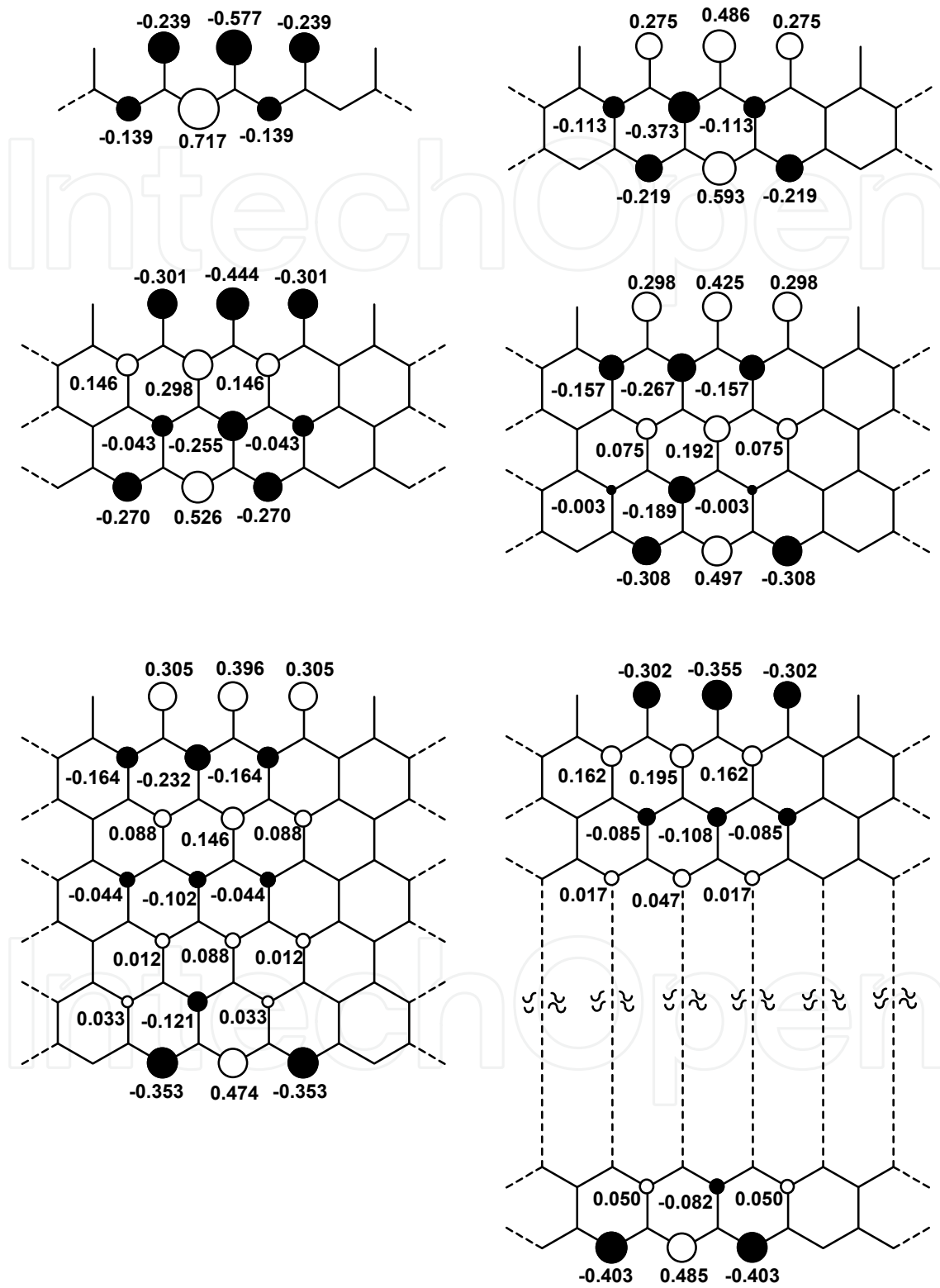


Fig. 3. Wannier functions of one-sided Klein edges with the number of ladders  $n=0, 1, 2, 3, 5,$  and  $10$ .

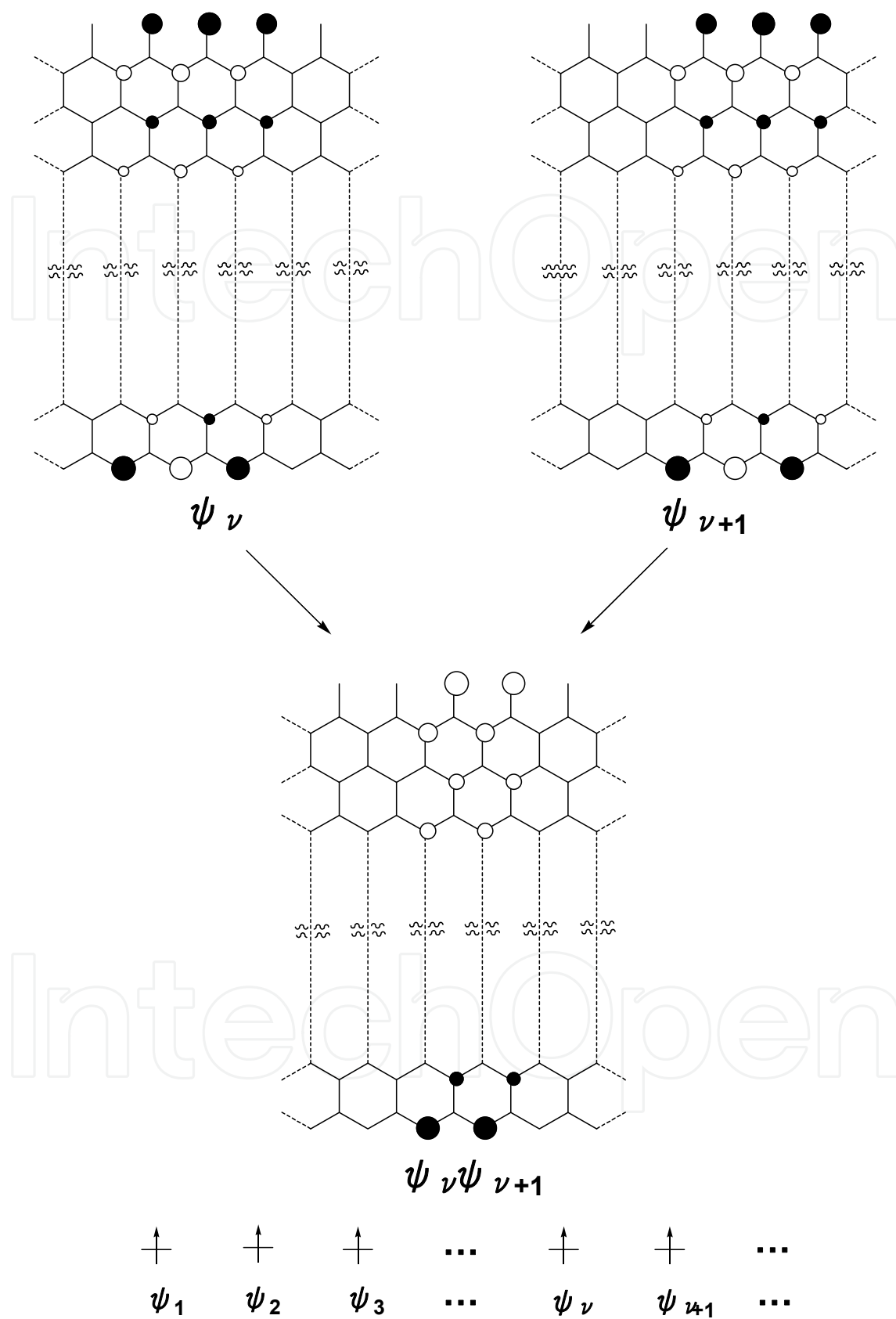


Fig. 4. Construction of two-electron wavefunctions from adjacent Wannier functions of one-sided Klein edges.

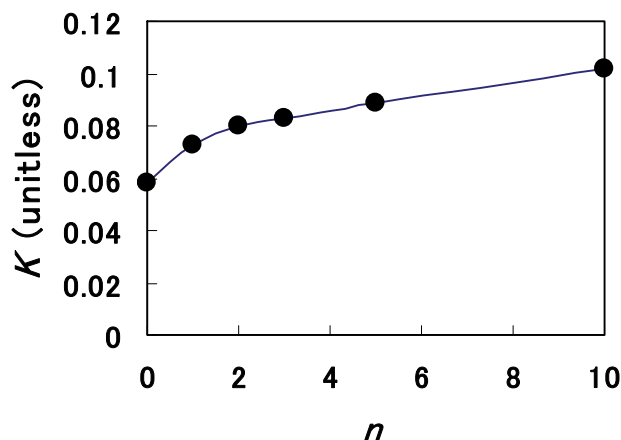


Fig. 5. Exchange integral  $K$  of one-sided Klein-edges per unit versus the number of ladders  $n$ .

### 3. Porous graphenes

Fig. 6 shows porous graphene. This compound was synthesized as a two-dimensional nanostructure (Bieri et al., 2009). They synthesized porous graphene by aryl-aryl coupling reactions on Ag (111) surface, and observed STM (scanning tunneling microscope) image of the honeycomb structures. In 2010, band structures of porous graphenes were investigated by several workers (Du et al., 2010; Hatanaka, 2010b; Li et al., 2010). The Hückel-level dispersion and DOS (density of states) are shown in Figs. 6 and 7 (Hatanaka, 2010b). The dispersion suggests semi-conductive band gaps, and the frontier bands are so flat as to be available for ferromagnetism. It is interesting that both HOCO and LUCO become flat at all the wavenumber region. Thus, this material is expected to show ferromagnetism when it is oxidized or reduced by proper dopants.

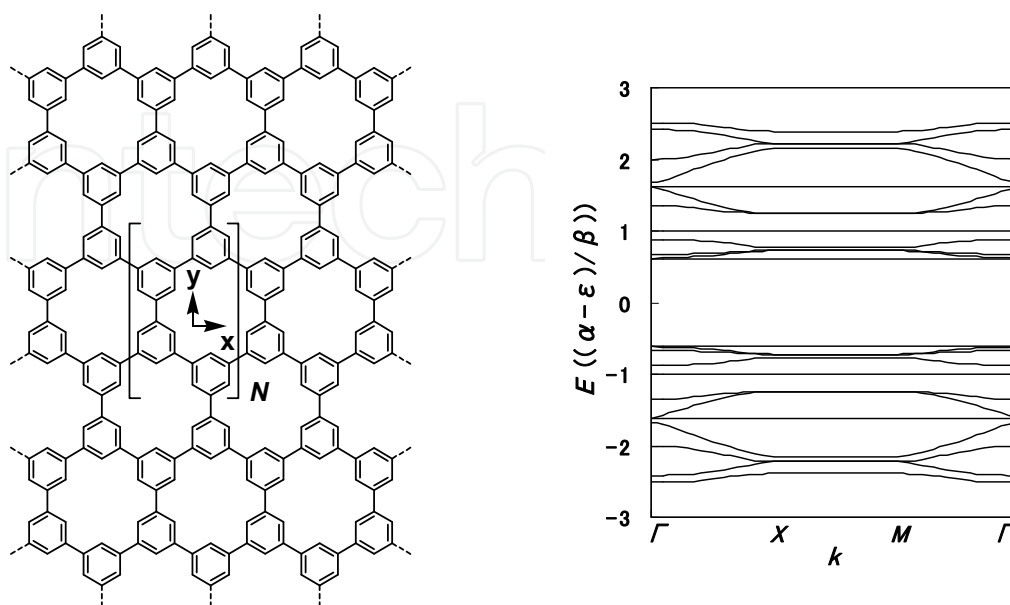


Fig. 6. Porous graphene and the dispersion based on Hückel level of theory.

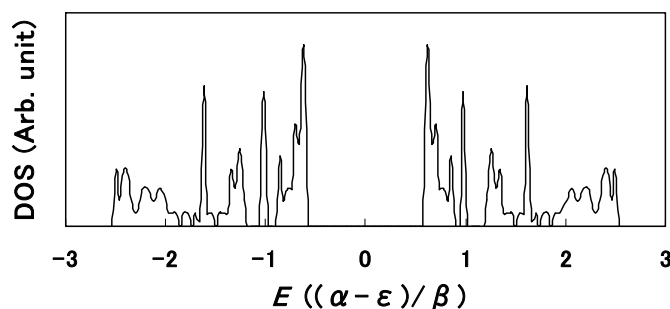


Fig. 7. DOS (density of states) of porous graphene based on Hückel level of theory.

The flat bands result from nodal character of phenylene units. Fig. 8 shows amplitude patterns of selected Hückel molecular orbitals of cyclohexa-*m*-phenylene, which is considered as a unit group in the porous graphene. We see that the HOMO and LUMO have nodes at each phenylene unit. Orbital interactions between node-node linkages are zero within the Hückel approximation. Thus, both HOCO and LUCO in porous graphene become flat at the frontier levels. It is interesting that eigenvalues  $\epsilon$  of HOMO ( $a+0.618\beta$ ) and LUMO ( $a-0.618\beta$ ) in cyclohexa-*m*-phenylene are identical to those of butadiene. Indeed,

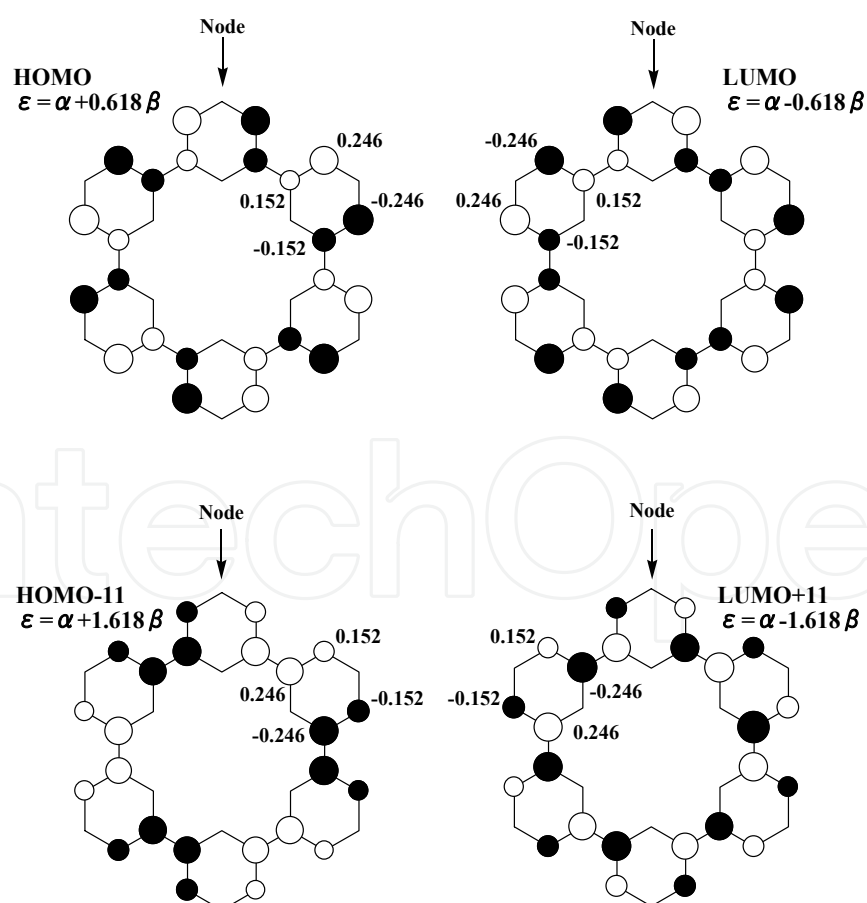


Fig. 8. Selected molecular orbitals of cyclohexa-*m*-phenylene. There are nodes at the peripheral sites.  $a$  and  $\beta$  are Coulomb and resonance integral, respectively.

apart from the normalization factors, amplitude patterns of butadiene's HOMO and LUMO spread between each phenylene unit. Moreover, eigenvalues of HOMO-11 ( $a+1.618\beta$ ) and LUMO+11 ( $a-1.618\beta$ ) of cyclohexa-*m*-phenylene are identical to those of the first and fourth orbitals in butadiene. These orbitals also cause flat bands in porous graphene at eigenvalues ( $a\pm 1.618\beta$ ). In porous graphene, additional flat bands coincidentally appear at eigenvalues ( $a\pm 1.000\beta$ ). These bands come from nodal character of  $e_{1g}$  orbitals in each benzene fragment.

Porous graphene ribbons with various edges are also of interest, despite the coupling directions are not unique and some defects of the coupling reactions may cause diversity of molecular-weight distribution. Fortunately, it has been proved that the frontier non-bonding level of any porous oligomer is invariant with respect to molecular weight and/or coupling direction due to the zero-overlap interactions of the phenylene units. Thus, porous graphenes including porous ribbons are promising precursors toward organic ferromagnets.

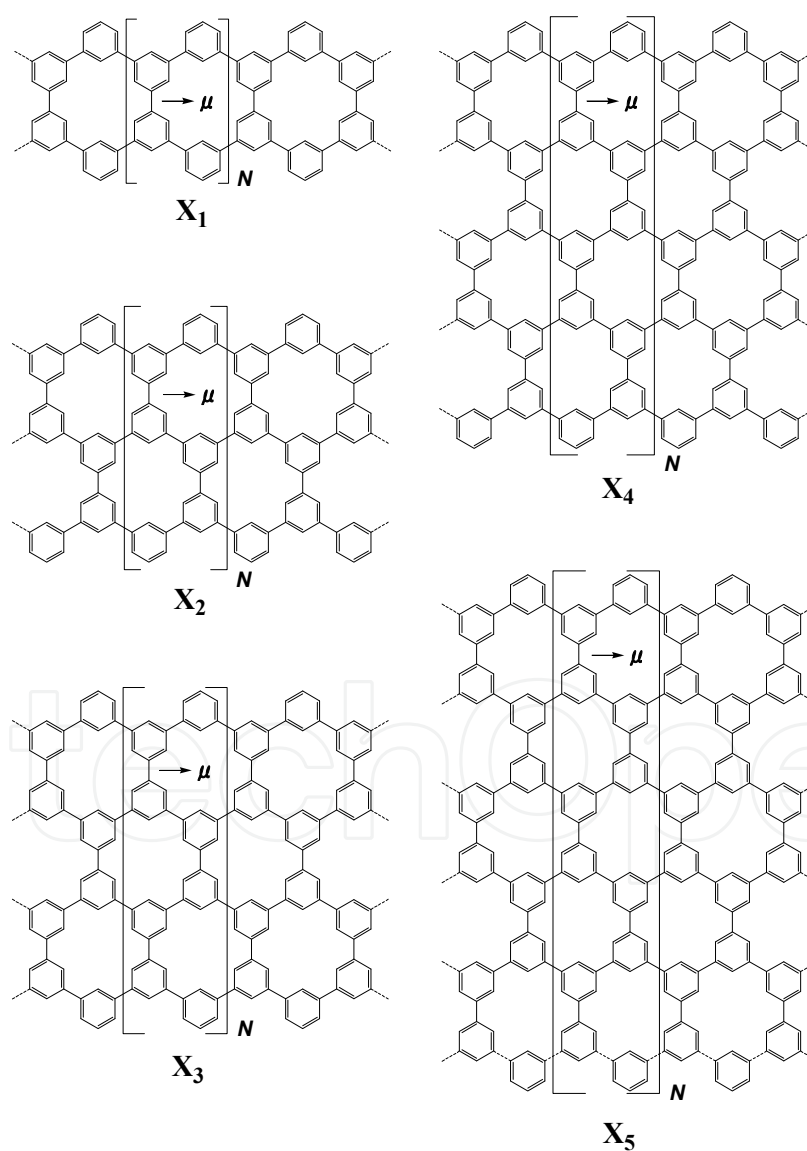


Fig. 9. Porous graphene ribbons  $X_n$  ( $n=1-5$ ) with  $n$  ladders cut along the  $x$  axis.  $\mu$  is the lattice vector.

Porous structures including boron and/or nitrogen are also interesting in that the hetero atoms serve as dopants, which increase or decrease the number of electrons in the frontier levels.

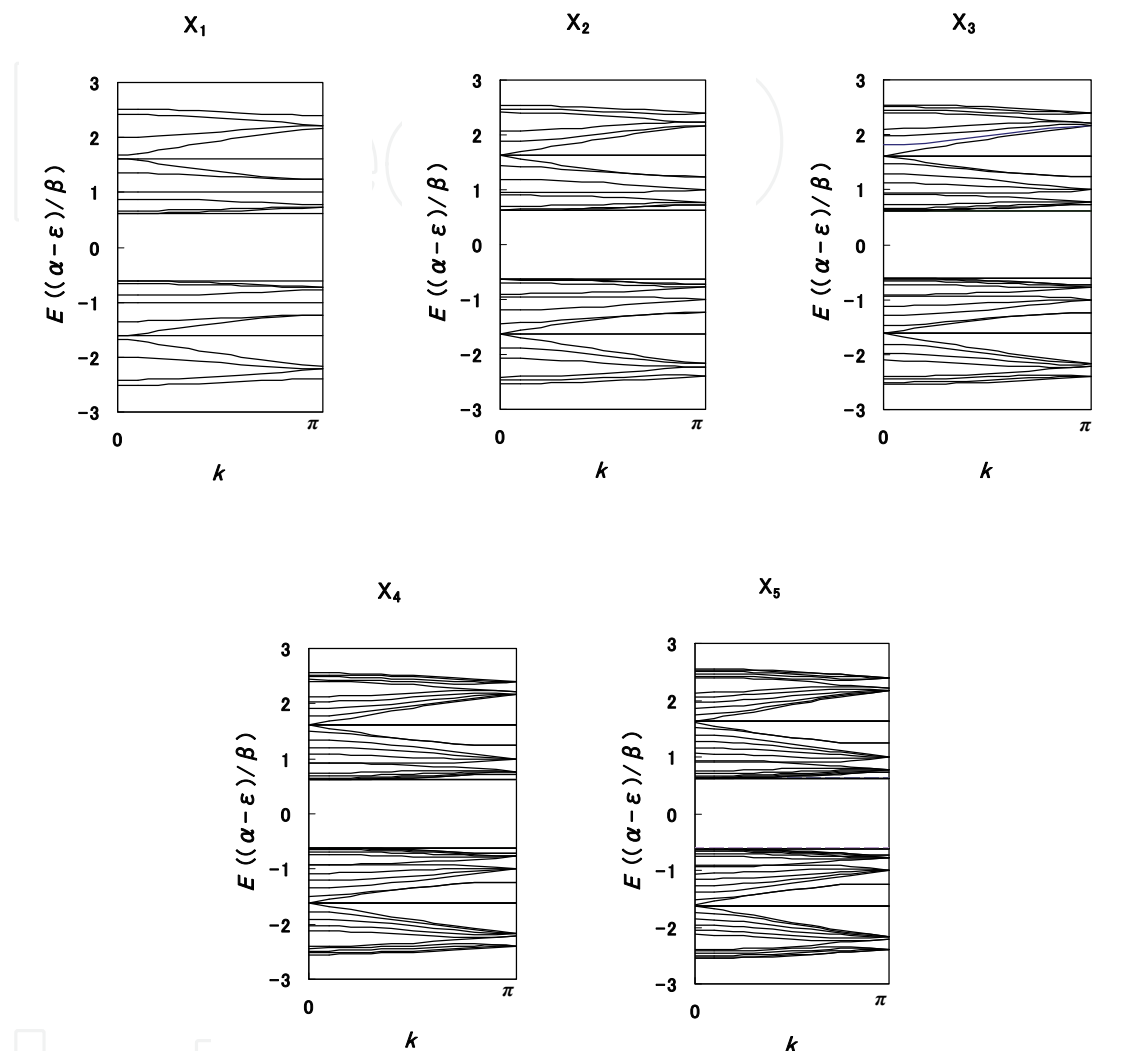


Fig. 10. Dispersions of  $X_n$  ( $n=1-5$ ) under Hückel level of theory.

Fig. 9 shows porous graphene ribbons cut along the  $x$  axis. The systems are classified by the number of porous ladders  $n$ , as denoted as  $X_1$ - $X_5$ . The edges have bay areas consisting of seven carbon atoms, and resemble acene edges of conventional graphene. Fig. 10 shows dispersion of  $X_1$ - $X_5$ . We see that the HOCOs and LUCOs are completely flat, similar to the two-dimensional porous graphene. Flat bands at  $(\pm 1.618\beta)$  are also conserved due to the nodal character of phenylene units. Interestingly, HOCOs and LUCOs in each system are  $n$ -fold degenerate, respectively. That is, HOCO and LUCO in  $X_1$  are single flat bands, and HOCO and LUCO in  $X_2$  are doubly degenerate. Similarly, three-, four-, and five-fold degenerate HOCOs and LUCOs appear in  $X_3$ ,  $X_4$ ,  $X_5$ , respectively. These degeneracies come from the systematic increase of the porous ladders. The resultant flat bands are also available for possible ferromagnetic interactions.

Fig. 11 shows porous graphene ribbons cut along the  $y$  axis. The systems are also classified by the number of porous ladders  $n$ , as denoted as  $Y_1$ - $Y_5$ . The edges have bay areas consisting of twelve carbon atoms, and resemble so-called phenanthrene edges of conventional graphene. Fig. 12 shows dispersion of  $Y_1$ - $Y_5$ . The HOCOs and LUCOs are completely flat, similar to  $X_1$ - $X_5$ . Flat bands at  $(a \pm 1.618\beta)$  also appear. HOCOs and LUCOs in each system are also  $n$ -fold degenerate, respectively.

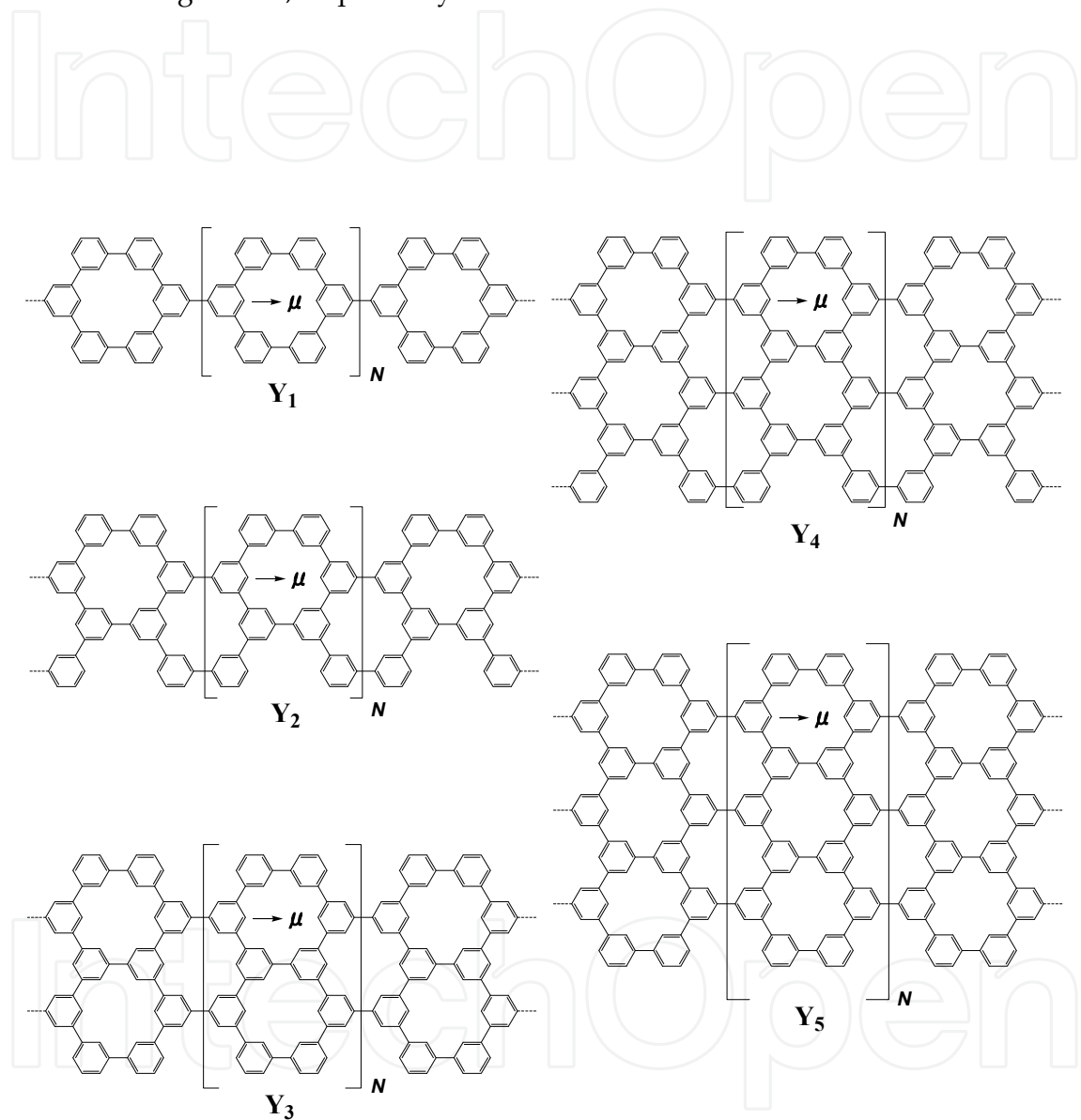


Fig. 11. Porous graphene ribbons  $Y_n$  ( $n=1-5$ ) with  $n$  ladders cut along the  $y$  axis.  $\mu$  is the lattice vector.

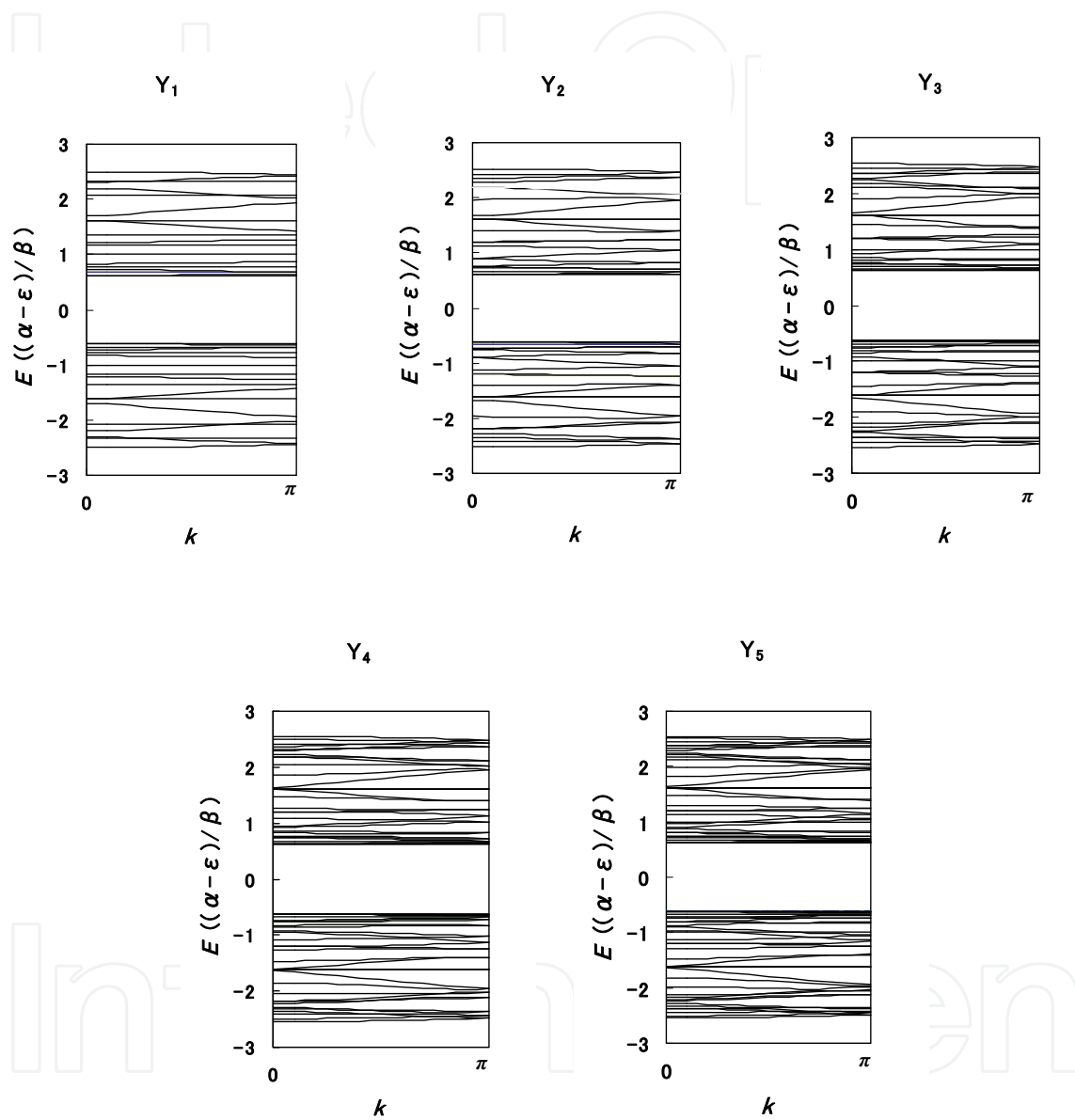


Fig. 12. Dispersions of  $Y_n$  ( $n=1-5$ ) under Hückel level of theory.

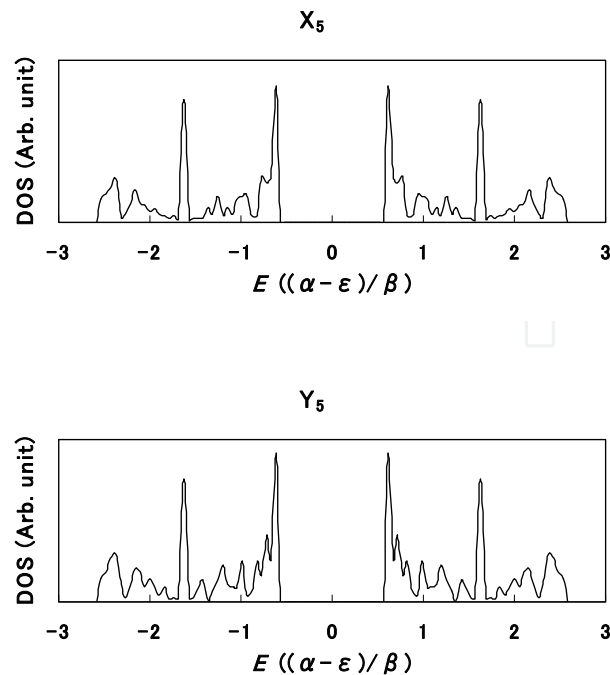


Fig. 13. DOS of  $X_5$  and  $Y_5$  under Hückel level of theory.

Fig. 13 shows DOS of  $X_5$  and  $Y_5$ . There are main peaks corresponding to the flat bands. The largest peaks are due to the systematic degeneracies of HOCOs and LUCOs, and thus, photoelectron spectroscopy experiments will give a major peak at ca. 9.1 eV. Theoretical predictions on the magnetism of porous graphenes await experimental confirmations.

#### 4. Defective graphenes

Recently, ferromagnetism of HOPG (highly oriented pyrolytic graphite) was found at room temperature (Červenka, et al., 2009; Esquinazi & Höhne, 2005; Mombrú et al., 2005). HOPGs often have defects, which form grain boundaries between the polycrystals. Laterally and longitudinally slipped defects in acene-edged HOPGs are particularly interesting in that the resultant defects are analyzable by graphene-based model (Hatanaka, 2010c). Fig. 14 shows definition of defects, in which the lateral and longitudinal displacements are represented by  $\Delta x$  and  $\Delta z$ . Fig. 15 shows extended-Hückel dispersion of acene-edged graphenes with laterally and longitudinally slipped defects. The number of honeycomb ladders is fixed to be 19. The bold lines and dotted lines represent  $\pi$  and  $\sigma$  bands, respectively. In laterally slipped defects ( $\Delta x > 0$ ), flatness of the frontier bands is lost with increase in the displacements, and the resultant double occupation of electrons leads to antiferromagnetic ground state. On the other hand, in longitudinally slipped defects ( $\Delta z > 0$ ), flatness of the frontier bands is conserved even if the displacement becomes infinity, and the resultant electronic state resembles that of polycarbene, in which  $\pi$  and  $\sigma$  spins coexist with ferromagnetic interactions.

Here we consider simple models of defects by using graphene ribbons with 3 ladders. Fig. 16 shows change of orbital pattern for the laterally slipped graphenes. We note that the effective displacement of lateral slip is smaller than the lattice period  $a$ . Frontier Bloch functions (HOCO and LUCO at  $k = \pi/a$ ) of non-distorted graphene is localized at the edges (Fig. 16a), and contact at  $k = \pi/a$ .  $\pi$ -Frontier Bloch functions in laterally slipped graphene are doubly degenerate and also contact at  $k = \pi/a$  under all the displacements (Fig. 16b). The amplitudes are localized inside the fault as well as at the acene edges. With increase in the lateral displacement, there appears a peculiar  $\sigma$  band, of which amplitude is shown in Fig. 16c. We see that this band consists of weak interacted dangling bonds in the slipped fault. The weak interaction causes crossing of frontier bands, as shown in the middle of Fig. 15, and thus, the magnetism due to acene-edged graphenes is considered to disappear.

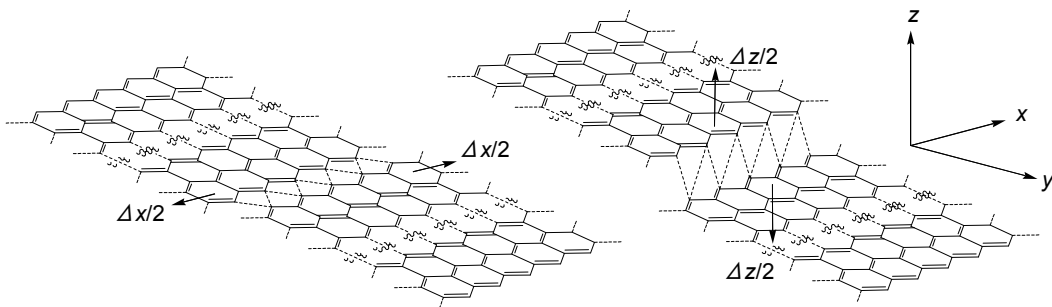


Fig. 14. Laterally and longitudinally slipped defective graphenes.

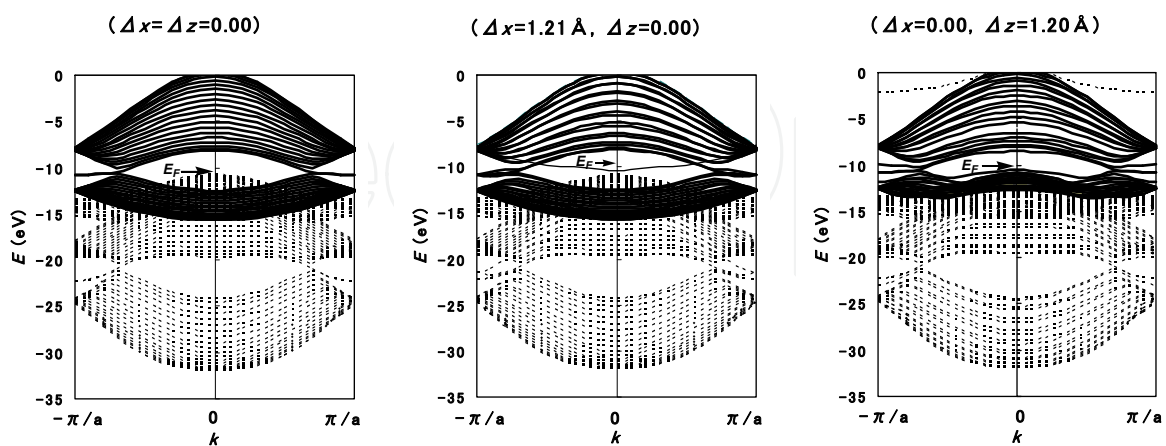


Fig. 15. Dispersion of defective graphenes based on extended Hückel level of theory.  $E_F$  is the Fermi levels.

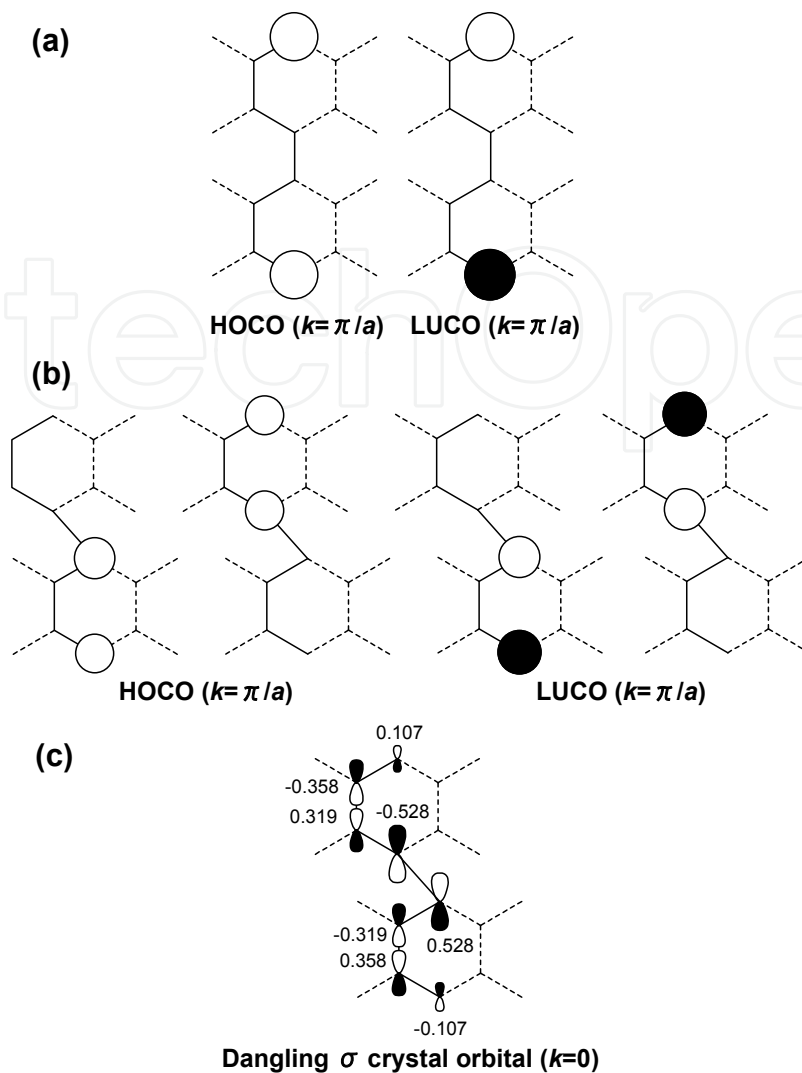


Fig. 16. Selected Bloch functions of acene-edged graphene with laterally slipped faults. (a)  $\Delta x=0$ , HOCO and LUCO at  $k=\pi/a$ , (b)  $\Delta x=1.21 \text{ \AA}$ , HOCOs and LUCOs at  $k=\pi/a$ , and (c)  $\Delta x=1.21 \text{ \AA}$ , dangling  $\sigma$  crystal orbital at  $k=0$ .

Fig. 17 shows  $\pi$ -frontier Bloch functions of longitudinally slipped graphene. Contrary to the laterally slipped graphene, amplitudes of the HOCO and LUCO always spread at the edges, and thus, their dispersions contact at  $k=\pi/a$  (Fig. 17a). When the longitudinal displacement becomes large, carbene-type  $\sigma$  bands also appear at the frontier level (Fig. 17b). These orbitals accommodate magnetic electrons of the carbene sites, and thus, longitudinally displacement causes another type of magnetism within the fault. This is considered to be the reason why HOPGs often exhibit weak ferromagnetism. When the displacement is small, it has been shown that energy cost for longitudinal slip is smaller than that of lateral slip (Hatanaka, 2010c), and the energy cost is perhaps compensated by the high-spin stability. Thus, as rough estimation, we guess that ferromagnetism observed in HOPGs is attributed to longitudinally slipped defects, which form grain boundaries including multilayers of graphene planes. Indeed, topographies corresponding to the longitudinally slipped defects were recorded in HOPGs by AFM (atomic force microscope) and MFM (magnetic force microscope) techniques (Červenka et al., 2009).

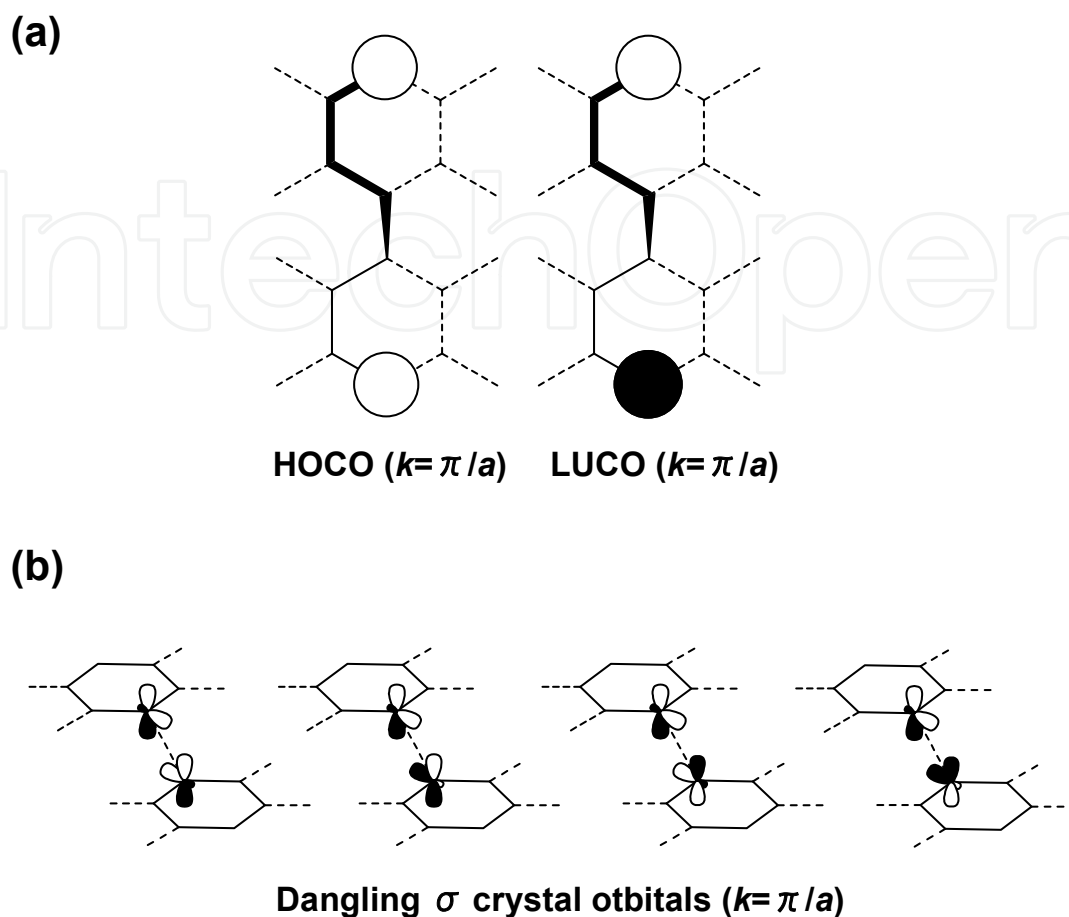


Fig. 17. Selected Bloch functions of acene-edged graphene with longitudinally slipped faults. (a)  $\Delta z=1.20 \text{ \AA}$ , HOCO and LUCO at  $k=\pi/a$ , and (b)  $\Delta z \rightarrow \infty$ , dangling  $\sigma$  crystal orbitals at  $k=\pi/a$ .

## 5. Conclusion

Some graphene-based ferromagnets were analyzed in view of their electronic states. There appear flat bands at the frontier levels, in which the Wannier functions span common atoms between the adjacent cells. If geometry conditions such as edges, pores, and defects are well controlled by chemical modification, graphene-based ferromagnets will be realized through the flat bands. Amplitudes of the Wannier functions have non-bonding character, and the frontier electrons are itinerant around each central cell. The degeneracy of frontier flat bands and the positive exchange integrals play key roles for ferromagnetic interactions of graphene-based ferromagnets.

## 6. Acknowledgements

Thanks are due to Elsevier B. V. for permission to use figures in the original papers (Hatanaka 2010a, 2010b, 2010c).

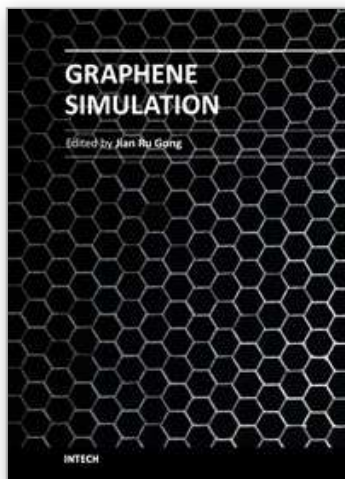
## 7. References

- Bieri, M; Treier, M; Cai, J; Ait-Mansour, K; Ruffieux, P; Gröning, O; Gröning, P; Kastler, M; Rieger, R; Feng, X; Müllen, K & Fasel, R. (2009). Porous graphenes: two-dimensional polymer synthesis with atomic precision. *Chemical Communications*, pp. 6919-6921
- Červenka, J; Katsnelson, M. I & Flipse, C. F. J. (2009). Room-temperature ferromagnetism in graphite driven by two-dimensional networks of point defects. *Nature Physics*, Vol. 5, pp. 840-844
- Du, A.; Zhu, Z & Smith, S. C. (2010). Multifunctional porous graphene for nanoelectronics and hydrogen storage: New properties revealed by first principle calculations. *Journal of the American Chemical Society*, Vol. 132, pp. 2876-2877
- Esquinazi, P & Höhne, R. (2005). Magnetism in carbon structures. *Journal of Magnetism and Magnetic Materials*, Vol. 290-291, pp. 20-27.
- Fujita, M; Wakabayashi, K; Nakada, K & Kusakabe, K. (1996). Peculiar localized state at zigzag graphite edge. *Journal of the Physical Society of Japan*, Vol. 65, pp.1920-1923
- Hatanaka, M. (2010a). Wannier analysis of magnetic graphenes. *Chemical Physics Letters*, Vol. 484, pp. 276-282
- Hatanaka, M. (2010b). Band structures of porous graphenes. *Chemical Physics Letters*, Vol.488, pp. 187-192
- Hatanaka, M. (2010c). Band structures of defective graphenes. *Journal of Magnetism and Magnetic Materials*, Vol. 323, pp. 539-546
- Hatanaka, M. (2011). Stability criterion for organic ferromagnetism. *Theoretical Chemistry Accounts*, Vol. 129, pp. 151-160
- Hatanaka, M. & Shiba, R. (2007). Ferromagnetic interactions in non-Kekulé polymers. *Bulletin of the Chemical Society of Japan*, Vol. 80, pp. 2342--2349
- Klein D. J. (1994). Graphitic polymer stripes with edge states. *Chemical Physics Letters*, Vol. 217, pp. 261-265
- Klein D. J. & Bytautas L. (1999). Graphitic edges and unpaired  $\pi$ -electron spins. *The Journal of Physical Chemistry A*, Vol. 103, pp. 5196-5210
- Kusakabe, K & Maruyama, M. (2003). Magnetic nanographite. *Physical Review B*, Vol. 67, pp. 092406-1-4
- Li, Y.; Zhou, Z.; Shen, P. & Chen, Z. (2010). Two-dimensional polyphenylene: experimentally available porous graphene as a hydrogen purification membrane. *Chemical Communications*, pp. 3672-3674
- Maruyama, M & Kusakabe, K. (2004). Theoretical predication of synthesis methods to create magnetic nanographite. *Journal of the Physical Society of Japan*, Vol. 75, pp.656-663
- Mombrú, A. W; Pardo, H; Faccio, R; de Lima, O. F; Leite, E. R; Zanelatto, G; Lanfredi, A. J. C; Cardoso, C. A. & Araújo-Moreira, F. M. (2005). Multilevel ferromagnetic behavior of room-temperature bulk magnetic graphite. *Physical Review B*, Vol. 71, pp.100404(R)-1-4

- Novoselov, K. S; Geim, A. K; Morozov, S. V; Jiang, D; Zhang, Y; Dubonos, S. V; Grigorieva, I. V. & Firsov, A. A. (2004). Electronic field effect in atomically thin carbon films. *Science*, Vol. 306, pp. 666-669
- Novoselov, K. S; Geim, A. K; Morozov, S. V; Jiang, D; Katsnelson, M. I; Grigorieva, I. V.; Dubonos, S. V. & Firsov, A. A. (2005). Two-dimensional gas of massless Dirac fermions in graphene. *Nature*, Vol. 438, pp. 197-200

IntechOpen

IntechOpen



### **Graphene Simulation**

Edited by Prof. Jian Gong

ISBN 978-953-307-556-3

Hard cover, 376 pages

**Publisher** InTech

**Published online** 01, August, 2011

**Published in print edition** August, 2011

Graphene, a conceptually new class of materials in condensed-matter physics, has been the interest of many theoretical studies due to the extraordinary thermal, mechanical and electrical properties for a long time. This book is a collection of the recent theoretical work on graphene from many experts, and will help readers to have a thorough and deep understanding in this fast developing field.

#### **How to reference**

In order to correctly reference this scholarly work, feel free to copy and paste the following:

Masashi Hatanaka (2011). Electronic States of Graphene-Based Ferromagnets, Graphene Simulation, Prof. Jian Gong (Ed.), ISBN: 978-953-307-556-3, InTech, Available from:

<http://www.intechopen.com/books/graphene-simulation/electronic-states-of-graphene-based-ferromagnets>

# **INTECH**

open science | open minds

#### **InTech Europe**

University Campus STeP Ri  
Slavka Krautzeka 83/A  
51000 Rijeka, Croatia  
Phone: +385 (51) 770 447  
Fax: +385 (51) 686 166  
[www.intechopen.com](http://www.intechopen.com)

#### **InTech China**

Unit 405, Office Block, Hotel Equatorial Shanghai  
No.65, Yan An Road (West), Shanghai, 200040, China  
中国上海市延安西路65号上海国际贵都大饭店办公楼405单元  
Phone: +86-21-62489820  
Fax: +86-21-62489821

© 2011 The Author(s). Licensee IntechOpen. This chapter is distributed under the terms of the [Creative Commons Attribution-NonCommercial-ShareAlike-3.0 License](#), which permits use, distribution and reproduction for non-commercial purposes, provided the original is properly cited and derivative works building on this content are distributed under the same license.

IntechOpen

IntechOpen